Available online at www.sciencedirect.com
ScienceDirect
Journal of Sound and Vibration 304 (2007) 154–174
JOURNAL OF SOUND AND VIBRATION
www.elsevier.com/locate/jsvi

Evaluation of modal density, radiation efficiency and acoustic response of longitudinally stiffened cylindrical shell

P. Ramachandran[a,*], S. Narayanan[b]

[a]*ENTEST, RCI, Hyderabad 50069, India*
[b]*Department of Mechanical Engineering and Dean, Academic Research, IIT, Madras, Chennai 600 036, India*

Received 8 February 2006; received in revised form 3 November 2006; accepted 7 February 2007

Abstract

An analytical method has been developed for predicting the modal density and the radiation efficiency of longitudinally stiffened cylinder to use in statistical energy analysis (SEA). In the present analysis, the stiffeners are treated as discrete elements and the natural frequencies and the mode shapes are calculated using the energy method. The modal density and the radiation efficiency are predicted from the derived natural frequencies and the mode shapes. The predicted values are compared with experimental measurements over a wide frequency range up to 10 kHz and the results are found to have good agreement except at low frequencies, where the individual global modes dominate the response. A correction factor is introduced in the estimation of radiation efficiency in the low-frequency range for unbaffled finite length cylinder. A statistical process has been evolved by considering an ensemble of 32 similar structural models with material and geometrical properties varying by $\pm 5\%$ over the nominal values to account for the uncertainties in the structure. For the assumed stiffened cylinder, the effect of the shapes of the stiffeners is found to have a small influence on the modal density and the radiation efficiency. As the number of stiffeners is increased beyond 32, a single term solution by neglecting the cross-coupling of various circumferential modes yields moderately accurate results and resulting in considerable saving of computation time. The acoustic responses of unstiffened and stiffened cylinders are predicted using SEA and validated by experiments. The presented analytical method can be easily extended to non-periodically stiffened cylinders with different types, shapes and orientations of the stiffeners etc.

1. Introduction

Stiffened cylindrical shell structures are used extensively in the aerospace industry due to their lightweight constructions. These structures are excited by broadband acoustic noise in the frequency range of 10 kHz in most of their service life. The vibro-acoustic response of these structures due to acoustic excitation is of prime concern not only from the structural point of view but also from the hearing comfort of the passengers inside the cabin. Owing to the high-frequency content of the excitation source, statistical energy analysis (SEA) is widely used for predicting the responses. In SEA, only three parameters viz. modal density, coupling loss factor (CLF) and the dissipation loss factor (DLF) are required for response prediction. In this paper, a

*Corresponding author. Tel.: +91 40 24306684; fax: +91 40 24306261.
E-mail address: p_rams@yahoo.com (P. Ramachandran).

0022-460X/$ - see front matter © 2007 Elsevier Ltd. All rights reserved.
doi:10.1016/j.jsv.2007.02.020

method for predicting the modal density and the radiation efficiency (which is proportional to the CLF) of axially stiffened cylindrical shell structure is developed. The results obtained by this method are verified experimentally.

The study of modal density of unstiffened cylinders has been carried out by many authors [1–7]. However, very few literature is available for the prediction of modal density of stiffened cylindrical shells either analytically or experimentally. Maymon [8] obtained the modal densities of stiffened shell structures by smearing the stiffeners over the whole surface of the shells and studied the effect of the stiffener eccentricities. He concluded that by stiffening with low area high eccentricity stiffeners, the modal density could be decreased to one-fourth of its normal value. Clarkson and Pope [9] assumed that the modal density of the stiffened shell would be equal to the sum of modal densities of shell, frame stiffeners and the ring stiffeners. However, he stated that the modal density might vary with the measurement location due to the stiffener effect. Williams and Banerjee [10] developed a numerical method for the calculation of natural frequencies of stiffened shell by considering the structure to be composed of a number of connected plates. Langley [11] derived the modal density of periodically stiffened beam and plate structures in terms of phase constants, which were associated with propagating wave motion. He showed that the modal density of a periodic structure was zero in a stop band and that the pass band average modal density was not affected by the imperfection in the attachment. Finnvedan [12] used wave-guide finite element method (FEM) to calculate the wave propagation characteristics for built up thin-walled structures. He explained the process of deriving the modal density and group velocity from FEM input for a beam structure.

The radiation efficiencies of simple plate and shell structures were examined by several authors like Cremer et al. [2], Manning and Maidanik [13], Szechenyi [4], Fahy [14] and Junger and Feit [15]. They derived the radiation efficiency on the basis of wave motion. Stepansishen [16,17] derived the radiation efficiency based on the Green's integral approach. Wang and Lai [18] studied the sound radiation efficiency of finite length, acoustically thick cylindrical shell using an analytical method validated by boundary element method (BEM). However, as stated earlier, only very few papers are available on the radiation efficiency of the stiffened cylinder. Laulagnet and Guyader [19] derived an expression for the radiation efficiency of the ring stiffened cylinder. They concluded that stiffening did not appear to be an effective tool to reduce the sound radiation below the critical frequency but some beneficial effects could be obtained in certain frequency ranges by locating driving forces on the stiffeners and by the selective orientation of excitation direction. All the above studies indicate that very little attention is given to the study of SEA parameters of stiffened shells. Hence, an attempt has been made to investigate the modal density and radiation properties of stiffened cylindrical structure.

The present paper is based on Mead and Bardell [20] who studied the free vibration of simply supported periodically stringer stiffened cylindrical shell using wave motion. They treated the stiffeners as discrete elements and considered only the single bay for finding out the natural frequencies using a graphical construction method in the wave propagation diagram. In the present study, the modal density and the radiation efficiency of a stiffened cylinder are obtained by solving an eigenvalue problem based on strain energies and kinetic energies of the total structure. The strain energy and kinetic energy expressions derived in the work of Mead and Bardell [20] are used to obtain the dynamic stiffness and mass matrices of the stiffened shell.

2. Theoretical prediction

2.1. Modal density

A thin cylindrical shell with thickness 'h', radius 'a' and length 'L' is considered for analysis in this paper. The middle surface of the shell is taken as the reference surface and cylindrical coordinate system (x,θ,z) is used. The x coordinate is taken in the axial direction where θ and z coordinates are, respectively, in the circumferential and radial directions of the cylindrical shell. u, v and w are the displacements of the middle surface of the cylinder in the x, θ and z directions, respectively. The geometry and coordinate systems are explained in Fig. 1. Simply supported boundary conditions are assumed in the analysis.

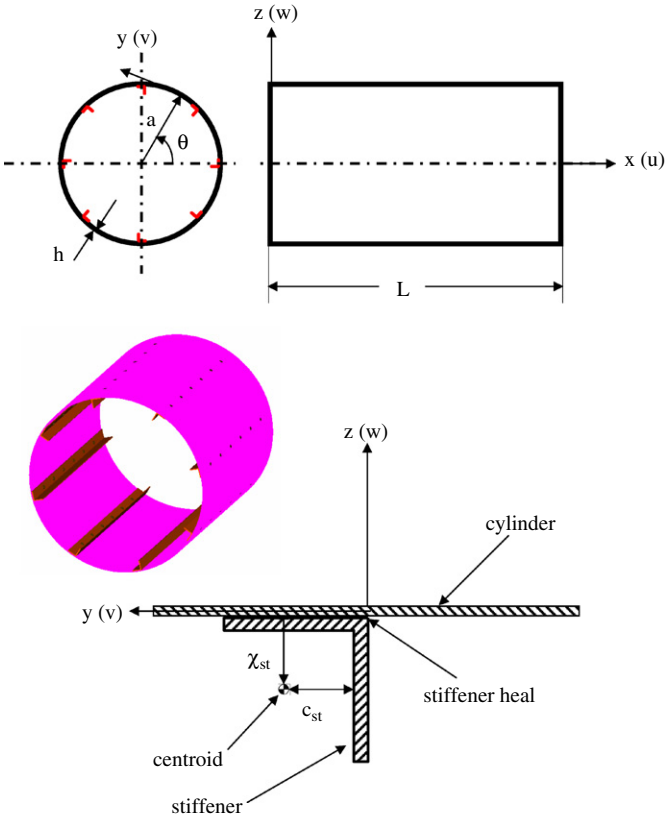

Fig. 1. Geometry and coordinate system of the cylindrical shell.

The strain energy U_s and the kinetic energy T_s of thin cylindrical shell according to Love [20] in the cylindrical coordinate system are given by

$$U_s = \int_0^{2\pi}\int_0^{L} \frac{Eh}{2(1-\mu^2)} \left\{ \begin{array}{l} \left(\frac{\partial u}{\partial x}\right)^2 + \frac{1}{a^2}\left(\frac{\partial v}{\partial \theta} + w\right)^2 + \frac{2\mu\partial u}{a\,\partial x}\left(\frac{\partial v}{\partial \theta} + w\right) + \frac{1}{2}(1-\mu)\left(\frac{\partial v}{\partial x} + \frac{1\partial u}{a\partial \theta}\right)^2 \\ + \frac{h^2}{12}\left[\begin{array}{l} \left(\frac{\partial^2 w}{\partial x^2}\right)^2 + \frac{1}{a^4}\left(\frac{\partial^2 w}{\partial \theta^2} - \frac{\partial v}{\partial \theta}\right)^2 \\ + \frac{2\mu\partial^2 w}{a^2\,\partial x^2}\left(\frac{\partial^2 w}{\partial \theta^2} - \frac{\partial v}{\partial \theta}\right) + \frac{2(1-\mu)}{a^2}\left(\frac{\partial^2 w}{\partial x\,\partial \theta} - \frac{\partial v}{\partial x}\right)^2 \end{array} \right] \end{array} \right\} a\,\mathrm{d}x\,\mathrm{d}\theta, \quad (1)$$

$$T_s = \frac{1}{2}\rho h \int_0^{2\pi}\int_0^{L} \left\{ \left(\frac{\partial u}{\partial t}\right)^2 + \left(\frac{\partial v}{\partial t}\right)^2 + \left(\frac{\partial w}{\partial t}\right)^2 \right\} a\,\mathrm{d}x\,\mathrm{d}\theta, \quad (2)$$

where E is the Young's modulus, μ the Poisson's ratio and ρ the density of the shell. The shear deformation and rotary inertia are neglected in the strain and kinetic energy calculations of the plain shell.

It is assumed that the axial stiffeners are treated as discrete elements with perfect attachment to the inner surface of the shell. When the displacements u, v, w and rotation $\partial w/\partial\theta$ of the shell are imposed at the heel, the

strain energy U_{st} and kinetic energy T_{st} of the stiffener are given by [20]

$$U_{st}=\frac{1}{2}\int_0^L E_{st}\left[\begin{array}{l}\left\{\begin{array}{l}A_{st}\left(\dfrac{\partial u}{\partial x}\right)^2+I_{yy}\left(\dfrac{\partial^2 w}{\partial x^2}\right)^2-2I_{yz}\left(\dfrac{\partial^2 w\partial^2 v}{\partial x^2\partial x^2}\right)+I_{zz}\left(\dfrac{\partial^2 v}{\partial x^2}\right)^2\\ \quad -2A_{st}\chi_{st}\dfrac{\partial u\partial^2 w}{\partial x\partial x^2}+2A_{st}c_{st}\dfrac{\partial u\partial^2 v}{\partial x\partial x^2}\end{array}\right\}\\ \quad +\dfrac{G_{st}J_{st}}{a^2}\left(\dfrac{\partial^2 w}{\partial x\,\partial\theta}\right)^2+\dfrac{E_{st}\Gamma_{st}}{a^2}\left(\dfrac{\partial^3 w}{\partial x^2\,\partial\theta}\right)^2\end{array}\right]\mathrm{d}x, \tag{3}$$

$$T_{st}=\frac{1}{2}\int_0^L \rho_{st}\left[\begin{array}{l}A_{st}\left\{\left(\dfrac{\partial u}{\partial t}\right)^2+\left(\dfrac{\partial v}{\partial t}\right)^2+\left(\dfrac{\partial w}{\partial t}\right)^2\right\}+I_{yy}\left\{\left(\dfrac{\partial^2 w}{\partial x\,\partial t}\right)^2+\dfrac{1}{a^2}\left(\dfrac{\partial^2 w}{\partial t\,\partial\theta}\right)^2\right\}\\ \quad +I_{zz}\left\{\left(\dfrac{\partial^2 v}{\partial x\,\partial t}\right)^2+\dfrac{1}{a^2}\left(\dfrac{\partial^2 w}{\partial\theta\,\partial t}\right)^2\right\}-2I_{yz}\dfrac{\partial^2 w}{\partial x\,\partial t}\dfrac{\partial^2 v}{\partial x\,\partial t}\\ \quad -2A_{st}\chi_{st}\left\{\dfrac{\partial^2 w}{\partial x\,\partial t}\dfrac{\partial u}{\partial t}+\dfrac{1}{a}\left(\dfrac{\partial^2 w}{\partial\theta\,\partial t}\right)\dfrac{\partial v}{\partial t}\right\}+2A_{st}c_{st}\left\{\dfrac{\partial^2 v}{\partial x\,\partial t}\dfrac{\partial u}{\partial t}+\dfrac{1}{a\partial\theta}\dfrac{\partial^2 w}{\partial t}\dfrac{\partial w}{\partial t}\right\}\end{array}\right]\mathrm{d}x, \tag{4}$$

where A_{st} is the area of cross-section, I_{yy}, I_{yz} and I_{zz} the moments of inertia about the heel point, E_{st} the Young's modulus, G_{st} the bulk modulus, ρ_{st} the density, Γ_{st} the warping constant of the stiffener, c_{st} and χ_{st} the horizontal and vertical distances, respectively, from the centroid of the stiffener to the heel of the stiffener. The geometrical details of the stiffener are illustrated in Fig. 1. In the formulation of strain energy, the axial deformation in the x direction due to stretching of the stiffener, flexural deformations due to bending in the z and θ directions and the shear deformations due to twisting about the stiffener heel are considered. Even though, the rotary inertia of the shell is neglected, the rotary inertia of the stiffener is included in the above kinetic energy expression.

The introduction of the axial stiffener causes the circumferential modes to be distorted. The following displacement field is considered for each axial mode m and distorted circumferential mode n [21]

$$\begin{aligned}u_{mn}&=\cos\left(\frac{m\pi x}{L}\right)\sum_{p=0}^{N}[U_{mn_p}(t)\cos p\theta+U'_{mn_p}(t)\sin p\theta],\\ v_{mn}&=\sin\left(\frac{m\pi x}{L}\right)\sum_{p=0}^{N}[V_{mn_p}(t)\sin p\theta+V'_{mn_p}(t)\cos p\theta],\\ w_{mn}&=\sin\left(\frac{m\pi x}{L}\right)\sum_{p=0}^{N}[W_{mn_p}(t)\cos p\theta+W'_{mn_p}(t)\sin p\theta],\end{aligned} \tag{5}$$

where U_{mn_p}, V_{mn_p} and W_{mn_p} are for symmetric modal amplitudes and U'_{mn_p}, V'_{mn_p} and W'_{mn_p} are for antisymmetric modal amplitudes and N is the maximum number of harmonic terms used in the circumferential direction.

Substituting the above displacement field into Eqs. (1)–(4) and by applying the Lagrange equation, the dynamic stiffness matrix $\mathbf{K}$ and mass matrix $\mathbf{M}$ of the complete cylinder can be written as

$$\begin{aligned}\mathbf{K}&=\mathbf{K}_s+\sum_1^q\mathbf{K}_{st},\\ \mathbf{M}&=\mathbf{M}_s+\sum_1^q\mathbf{M}_{st},\end{aligned} \tag{6}$$

where $\mathbf{K}_s$, $\mathbf{M}_s$ are, respectively, the stiffness and mass matrices of the cylinder and $\mathbf{K}_{st}$, $\mathbf{M}_{st}$ are, respectively, the stiffness and mass matrices of the each stiffener, and q is the number of axial stiffeners. The complete description and the elements of the matrices $\mathbf{K}_s$, $\mathbf{K}_{st}$, $\mathbf{M}_s$ and $\mathbf{M}_{st}$ are explained in Ref. [22]. The natural

frequencies ω and mode shapes $\{U\}$ are obtained by solving the eigenvalue problem:

$$[\mathbf{K}]\{\mathbf{U}\} = \omega^2[\mathbf{M}]\{\mathbf{U}\}. \tag{7}$$

The number of frequencies that lie in the frequency range of interest will give the mode count N_m and the modal density is given by

$$n(f_c) = \frac{N_m}{f_2 - f_1}, \tag{8}$$

where f_1, f_c and f_2 are the lower, center and upper frequencies of the frequency band of interest, respectively.

The above procedure yields a simple method for predicting the modal density of stiffened cylinder by a deterministic approach. However, in the high-frequency analysis, it is better to consider the behavior of an ensemble of similar systems with slightly different properties rather than a deterministic approach. This will account for the inherent uncertainties present in the physical and geometrical properties of similar structures due to fabrication, manufacturing and assembly variations. SEA models are treated as a base line representation of such populations of similar systems. A Monte Carlo test conducted by Huang and Radcliffe [23] on a simple SEA model having 3 subsystems showed that the theoretical Gaussian distributions would be good approximations for response distribution of a finite parameter SEA model. As per the central limit theorem, Gaussian distribution can be generated by combining a number of independent random variables having arbitrary distribution. In the present work, the material properties like Young's modulus, mass density and geometrical properties like cylinder radius, length, thickness, stiffener cross-sectional properties and the angular positions of the stiffeners are assumed to be uncorrelated, with uniform distributions having $\pm 5\%$ variations from their nominal mean value. The average value of modal density and radiation efficiency which are estimated using 32 such models are used for the prediction of acoustic response. Thus, the present method yields a statistical estimate of the parameters examined in this analysis.

2.1.1. Unstiffened cylinder

Using the above analytical method, the modal density of unstiffened steel cylinder is predicted first. The nominal mean value of the cylinder properties are assumed as

$$\text{Radius } (a) = 0.2515\,\text{m}, \quad \text{Length } (L) = 0.63\,\text{m},$$
$$\text{Thickness } (h) = 0.003\,\text{m}, \quad \text{Young's Modulus } (E) = 2.1 \times 10^{11}\,\text{N/m}^2,$$
$$\text{Density } (\rho) = 7820\,\text{kg/m}^3, \quad \text{Poisson's ratio } (\mu) = 0.3.$$

For the unstiffened cylinder, the circumferential modes of displacement field (5) are uncoupled and are given by

$$u_{mn} = \cos\left(\frac{m\pi x}{l}\right)\left[U_{mn}(t)\cos n\theta + U'_{mn}(t)\sin n\theta\right],$$
$$v_{mn} = \sin\left(\frac{m\pi x}{l}\right)\left[V_{mn}(t)\sin n\theta + V'_{mn}(t)\cos n\theta\right],$$
$$w_{mn} = \sin\left(\frac{m\pi x}{l}\right)\left[W_{mn}(t)\cos n\theta + W'_{mn}(t)\sin n\theta\right]. \tag{9}$$

Each cylindrical shell mode corresponds to a simple axial mode m and circumferential mode n having the same frequency for both symmetric and anti symmetric circumferential modes. By varying the axial mode m from 1 to 50 and n from 0 to 50, the natural frequency of each mode is estimated. From this, the minimum numbers of axial and circumferential modes required for 10 kHz band analysis are found to be 28 and 36, respectively. However, subsequent analysis has been carried out up to 50 axial modes and 50 circumferential modes to accommodate for the statistical variations in the material and geometrical properties as explained in the previous section.

One of the important frequencies of the cylinder is the ring frequency. At the ring frequency, the shell undergoes uniform expansion and contractions with $n = 0$ and the mode is termed as the breathing mode. At the ring frequency, the modal density of the cylinder would be high and a large number of modes coexist closer to this frequency. Beyond the ring frequency, the shell behaves like a flat plate with equal area. The theoretical

ring frequency of the unstiffened cylinder is given by [4]

$$f_r = \frac{C_L}{2\pi a} \quad \text{with} \quad C_L = \sqrt{\frac{E}{\rho(1-\mu^2)}}, \tag{10}$$

where C_L is the longitudinal wave speed on a flat plate. The ring frequency for the cylinder calculated by the above equation is 3438 Hz. In the present analysis, the ring frequency of the shell is assumed to be the frequency corresponding to the mode $m = n = 0$ and found to be the same as the theoretical ring frequency.

Using Eq. (8), the modal density of the unstiffened cylinder having nominal properties (single sample without any variation applied to its geometrical and material properties) is predicted first and compared with that obtained by Langley [6] for a constant bandwidth of 500 Hz in Fig. 2. The predicted results match well with the Langley's result. The Langley's method of estimating modal density is based on a statistical process whereas the currently predicted modal density is for a single sample. Hence, as explained in the earlier section, the material and geometrical properties of the cylinder are varied by $\pm 5\%$ over the nominal values with uniform distribution. The average modal density of 32 such stochastic models is estimated and plotted in the same Fig. 2. It can be seen that, the averaged estimation smoothens out the modal density curve, which is in very good agreement with Langley's result. This method of predicting modal density for the unstiffened cylinder based on a statistical estimate has been extended to the case of the stiffened cylinder.

2.1.2. *Stiffened cylinder*

Eight 'L'-type steel stiffeners of size 0.012 m × 0.012 m × 0.003 m are added to the unstiffened cylinder in the axial direction at equal angles. Using Eqs. (3)–(6), the dynamic stiffness and mass matrices of the stiffened cylinder are obtained for $N = 100$. Solving the eigenvalue problem represented by Eq. (7), the natural frequencies of stiffened shell are obtained and the modal density is calculated using Eq. (8). As mentioned earlier, 32 iterations are carried out by varying both cylinder and the stiffener material and geometrical properties and average modal density of the stiffened shell is shown in Fig. 3.

It is seen that, addition of axial stiffeners does not alter the ring frequency. The modal density curve of the stiffened cylinder is similar to that of the unstiffened cylinder modal density curve. For the present stiffened cylinder, the peak modal density is of the same order as that of the unstiffened cylinder and occurs at the ring frequency. However, above the ring frequency, the modal density of stiffened cylinder is higher than the unstiffened cylinder modal density. This may be due to the fact that most of the stiffened shell natural frequencies are lower than the unstiffened shell frequencies for the same axial and circumferential mode numbers and the difference in the modal frequencies between the stiffened and unstiffened cylinders increases as the frequency increases.

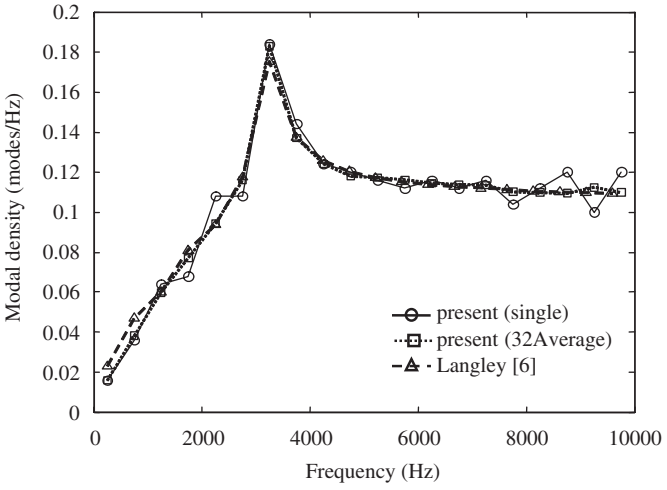

Fig. 2. Modal density of unstiffened cylinder.

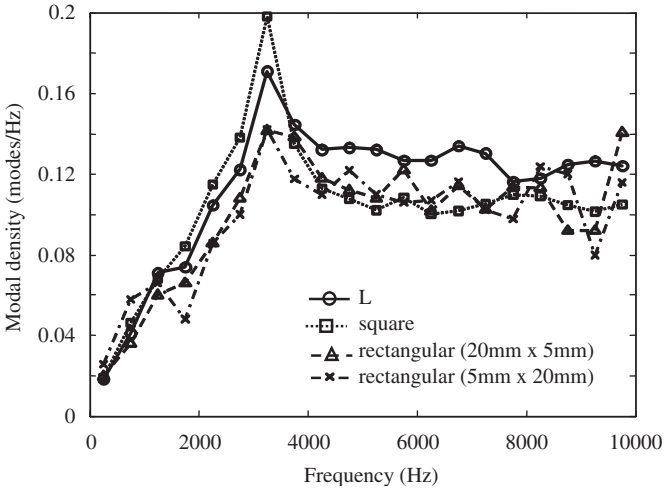

Fig. 3. Modal density of stiffened cylinder with different type of stiffeners.

Keeping the same cross-sectional area and the number of the stiffeners, the average modal densities are predicted for different types of stiffener cross-sections which are also shown in Fig. 3. The cylinder with square cross-section stiffeners has a higher modal density near the ring frequency as compared to that of the cylinders with other types of stiffeners. However, above the ring frequency, the modal density of cylinder with square stiffeners is generally lower than the modal densities of cylinders stiffened with other types of axial stiffeners.

Below the ring frequency, the size and shape of the stiffeners do not have much influence on the modal density. This may be due to the fact that, for lower order axial and circumferential modes below the ring frequency, the strain energy due to stretching is predominant than the strain energy due to bending and hence stiffeners are less effective for these modes. In Fig. 4, the symmetric and antisymmetric mode shapes and their corresponding frequencies of stiffened cylinder are compared for various predominant circumferential modes for two different axial modes. For the axial mode number $m = 1$, the frequencies f_a when the stiffeners are at antinodal lines (where the radial displacement would be maximum) are lower than the frequencies f_n when the stiffeners are at nodal lines (where the radial displacement would be minimum) of circumferential modes. For lower order axial modes, the stiffeners are less effective. The stiffened shell frequencies are lower than unstiffened shell frequencies.

However, above the ring frequency, the cylinder behaves as a flat panel and the predominant strain energy is due to bending. Hence, the position of the stiffeners on the circumferential direction is a major factor in controlling the frequency. When the predominant circumferential mode number n is an integer multiple of $q/2$ where q is the number of stiffeners, the stiffeners are positioned either at antinodal or nodal lines of circumferential modes. Since the stiffeners are more effective in bending, the frequency f_a is higher than the frequency f_n. Above the ring frequency, the circumferential mode number would be high for lower order axial modes. For higher order circumferential modes, there is a steep change in curvature and hence, the torsional rigidity of the stiffener is the other major factor in controlling the stiffened shell frequency. The square stiffener has moderately better flexural and torsional rigidity than the other type of stiffeners and hence the modal density of the shell with square stiffeners is lower than the other stiffened shells above the ring frequency.

Similarly keeping the same total cross-sectional area of all the stiffeners, the number of square stiffeners is varied to study the effect of coupling of circumferential modes on the modal density. The averaged modal densities of stiffened cylinders having 8, 32 and 128 square stiffeners are plotted in Fig. 5. In the same figure, the modal densities of the stiffened cylinders are compared with only one term displacement solution of Eq. (9), which neglects the cross-coupling between circumferential modes.

Below the ring frequency, the number of stiffeners does not have much influence on the modal density as mentioned in the previous case of different types of stiffeners. Near, the ring frequency, the modal density is maximum for cylinder with 8 stiffeners and minimum for cylinder with 32 stiffeners. However, above the ring

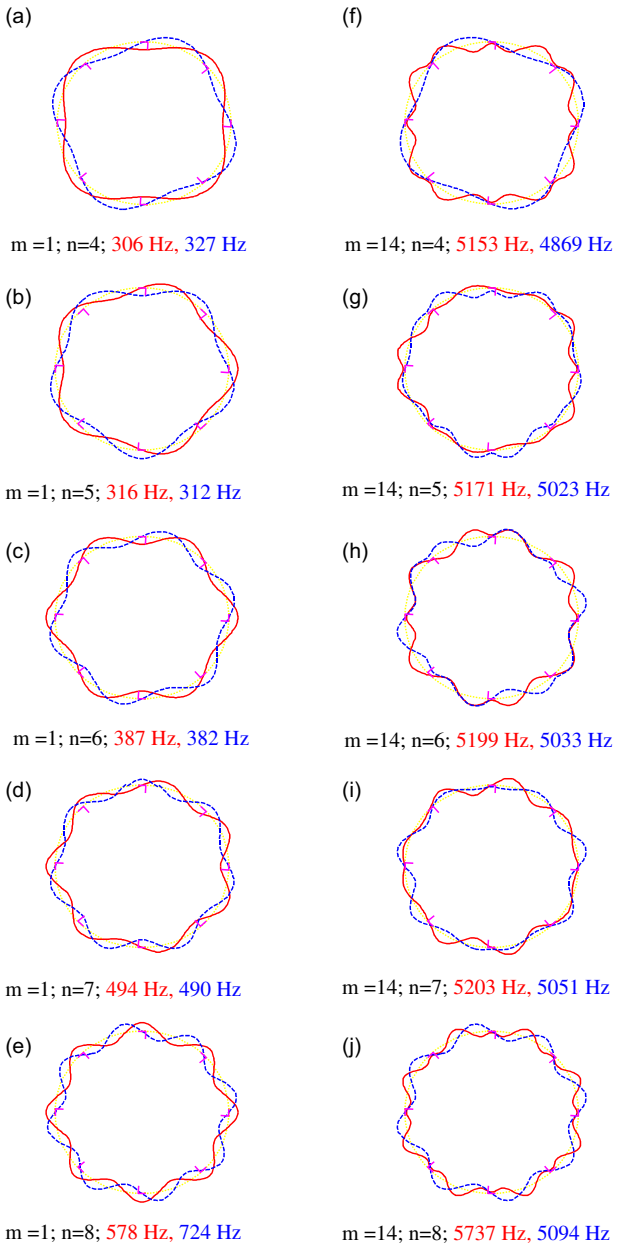

Fig. 4. Mode shape plots of stiffened cylinder: ——, symmetric mode; – – –, anti symmetric mode; · · · · · · ·, undeformed shell. The frequency values shown are for sym-metric and anti symmetric modes, respectively.

frequency the modal density increases as the number of stiffeners is increased. This may be due to the fact, that the bending and torsional rigidity of stiffeners decrease as the number of stiffeners is increased due to very low sectional properties (for maintaining the same total cross-sectional area of all stiffeners). From Fig. 5, it can be seen that one term solution using the displacement field of Eq. (9) is found to be moderately accurate when the number of stiffeners is equal to 32, but fits very well with multiterms solution when the stiffeners are more than 32. When the number of stiffeners is equal to 128, there is no difference in the modal density between multiterms and single term solutions. Hence, when the stiffeners are more than 32, single term solution can be used for predicting the modal density. The calculation becomes simple since the stiffness and mass matrices of the stiffened shell would be diagonal matrices. Hence, the eigenvalues of Eq. (7) can be obtained individually

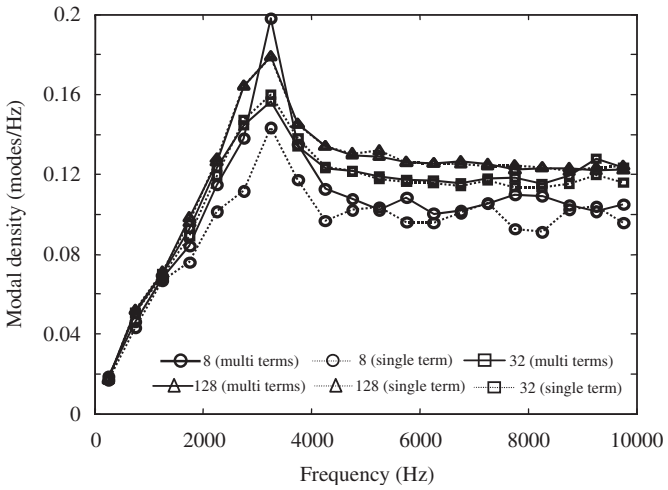

Fig. 5. Modal density of stiffened cylinder with different number of square stiffeners.

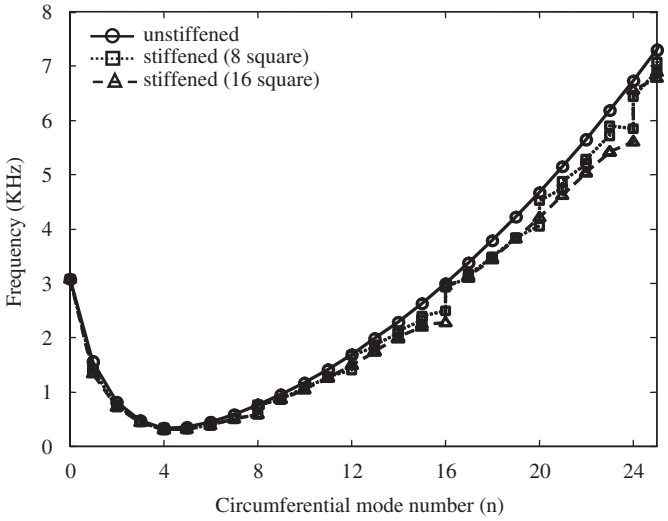

Fig. 6. Variation of frequency with circumferential mode number ($m = 1$).

for each m and n, which reduces the matrix size to be solved from one $6N \times 6N$ matrix to N independent matrices of size 6×6. When the number of stiffeners is more, the solution using smeared thickness as given by Maymon [8] also yields moderately accurate results. The single term solution results in considerable saving of computation time.

There will be stop bands and pass bands for periodically stiffened cylinders as discussed in Ref. [20]. In order to study the pass bands and stop bands, the variations of frequency with circumferential mode numbers for two different axial mode numbers of unstiffened and stiffened cylinders are plotted in Figs. 6 and 7. In these figures, the stiffened cylinders having 8 and 16 square sections with equal total cross-sectional area of the stiffeners are considered as in the previous case. Each circumferential mode will have two natural frequencies corresponding to symmetric and anti symmetric modes. The unstiffened cylinder shows smooth variation of the frequency for both axial modes $m = 1$ and 10. However, the plot for the stiffened cylinder shows jumps in the frequency axis when the circumferential mode number n is an integer multiple of $q/2$, where q is the number of stiffeners. These jumps are predominately seen in the higher-order axial mode $m = 10$ and these jumps are called as stop bands. The frequency range between two jumps are called as pass band and the number of

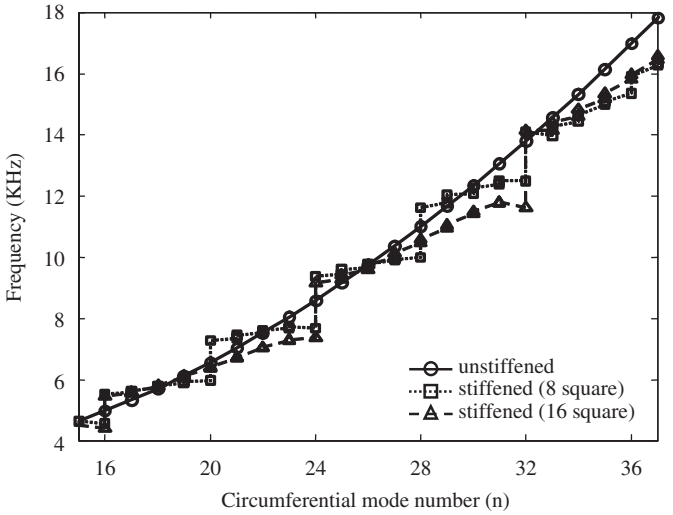

Fig. 7. Variation of frequency with circumferential mode number ($m = 10$).

frequencies in each pass band will be equal to the number of stiffeners [20], which can be verified in Figs. 6 and 7. As the axial mode number increases, the stop bandwidth increases, and all the circumferential modes in the pass band are grouped together and closely spaced in the frequency axis. As mentioned earlier, for the lower order axial mode $m = 1$, the stiffeners are not effective in bending and the frequencies of stiffened cylinder are less than unstiffened cylinder for the same circumferential mode, whereas for $m = 10$, the stiffeners are effective in controlling certain circumferential modal frequencies. Hence, the modal density of stiffened cylinder in Fig. 3 shows fluctuations in the high-frequency range even after averaging of 32 statistical models due to alternate stop and pass band effect.

2.2. Radiation efficiency

Radiation efficiency σ_{rad} is another important parameter in vibro-acoustic response prediction since this is the parameter, which links the vibrational energy in the structure due to acoustic excitation as well as the acoustic noise due to mechanical excitation. The relation between radiation efficiency and the CLF of structure to acoustic system is given by [13]

$$\text{CLF} = \frac{\sigma_{\text{rad}} \rho_a c}{2\pi f \mu_s}, \tag{11}$$

where ρ_a is the density of air, c the speed of sound in air and μ_s the surface mass density of the structure.

The radiation efficiency is calculated from the radiation resistance of each mode as illustrated by Stephanishen [17]. Only the self-radiation resistance of each mode is taken into account for the calculation of radiation efficiency. The spectrally averaged radiation efficiency of the structure in the frequency band of interest is the mean value of the radiation efficiencies of all the structural modes in that band. The average radiation efficiency of 32 stochastic models is calculated as in the case of modal density prediction.

2.2.1. Unstiffened cylinder

The radiation efficiency of the unstiffened steel cylinder is plotted in Fig. 8 in dB and compared with the expression given by Miller and Faulkner [24]. The predicted result matches well with their expression except in the very low-frequency region, below the critical frequency f_{cr} where

$$f_{\text{cr}} = \frac{\sqrt{3}c^2}{\pi h C_L}. \tag{12}$$

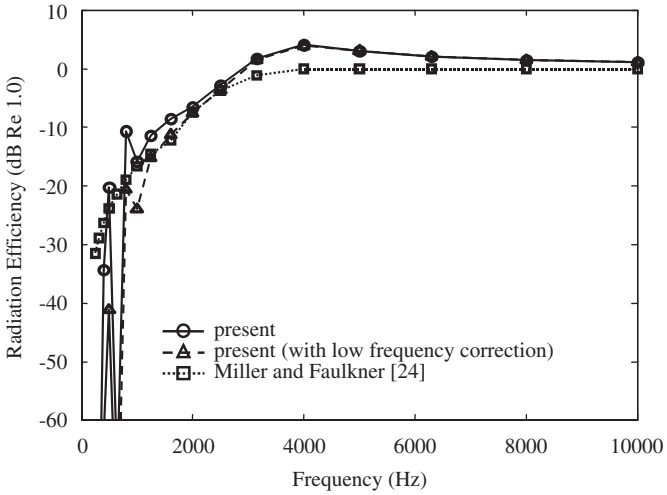

Fig. 8. Radiation efficiency of unstiffened cylinder.

At the critical frequency, the acoustic and structural wavelengths will be equal and the acoustic radiation will be high. In the present case, the critical frequency of the cylinder is equal to 3910.8 Hz.

Miller and Faulkner [24] assumed that the maximum radiation efficiency would be equal to 1. However as per [14–17,25], radiation efficiency will be slightly higher near the critical frequency. Hence, the radiation efficiency predicted using the present method shows values higher than 1 near the critical frequency and reduces to 1 as the frequency increases further.

At low frequency, a correction factor is applied as demonstrated by Oppenheimer and Dubowsky [26] to account for the radiation loss of the edge modes due to short circuiting of acoustic flow near the edges. The correction factor is applied only below the critical frequency of the cylinder and the corrected radiation efficiency is given by

$$\sigma_{\mathrm{rad}}^{\mathrm{cor}} = \sigma_{\mathrm{rad}} F_{\mathrm{edge}} F_{\mathrm{cyl}}, \tag{13}$$

where F_{edge} is the correction factor due to cross flow near the edges, which is given by [26]

$$F_{\mathrm{edge}} = \frac{49(f/f_c)^3}{\left(1 + 49(f/f_c)^3\right)} \tag{14}$$

and F_{cyl} is the correction factor that accounts for the effect of inertial flow that surrounds the cylinder at low frequencies where the acoustic wavelength exceeds the cylinder length and it is given by [26]

$$F_{\mathrm{cyl}} = \frac{53 f^4 A^4/c^4}{\left(1 + 53 f^4 A^4/c^4\right)}. \tag{15}$$

The corrected radiation efficiency plotted in Fig. 8 shows a reduction in the radiation efficiency below the critical frequency.

2.2.2. *Stiffened cylinder*

Similarly, the radiation efficiency of stiffened cylinder is calculated from the mode shape results obtained from Eq. (7). In the unstiffened cylinder, the circumferential modes are of simple harmonic waves whereas for stiffened cylinder these modes are distorted due to the influence of the stiffeners. In order to arrive at the circumferential mode number to be used in the radiation efficiency calculation for stiffened cylinder, the mode having predominant radial displacement component is considered. The predicted radiation efficiencies for various types of stiffeners are shown in Fig. 9. It can be seen that, the influence of the stiffeners on the radiation efficiency is insignificant when compared to the modal density variation, above the critical

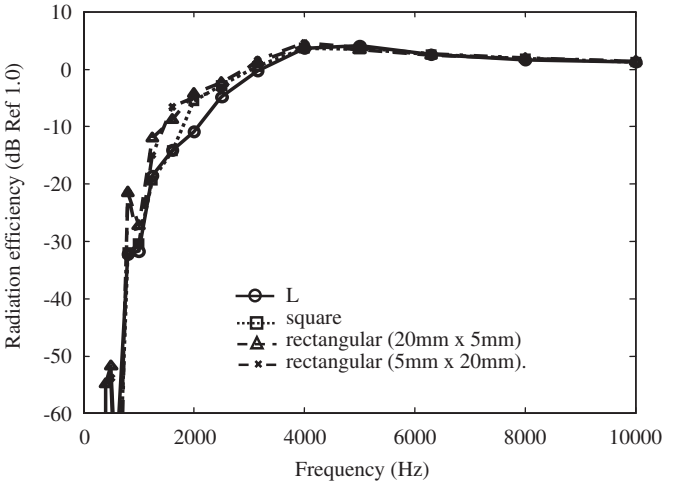

Fig. 9. Radiation efficiency of stiffened cylinder with different cross-sections.

frequency. The low-frequency correction is applied as explained in the unstiffened cylinder assuming the same critical frequency of the unstiffened cylinder.

3. Experimental verification

3.1. Modal density

In order to verify the analytical results obtained in the previous sections, experiments are carried out for modal density and radiation efficiency measurements. The geometry, material and other structural properties of the unstiffened cylindrical shell in the experiment are the same assumed for the simulation studies. The stiffened cylinder is fabricated by adding eight 'L'-type steel stiffeners with the size 0.012 m × 0.012 m × 0.003 m to the unstiffened cylinder. However, the cylinders are fitted with bulkhead on the both ends for suspension purpose and the weight of the bulkhead is not considered in the calculations of modal density and radiation efficiency. Each cylinder is suspended from the top bulkhead using bungee rope in a reverberation chamber as shown in Fig. 10 and excited laterally using electromagnetic shaker on the outer surface of the cylinder. A small size force transducer is kept in between the shaker and the cylinder to measure the input excitation level. A miniature accelerometer with built in preamplifier is placed on the inner surface of the cylinder exactly at the location of excitation to measure the point mobility. Another eight miniature accelerometers are mounted on the cylinder at random locations. Four microphones are suspended at different locations to measure the sound pressure level in the reverberation chamber. The cylinder is excited at 8 randomly selected locations by a random noise generator in the frequency range of 20 Hz to 12 kHz. The signals from the force transducer, accelerometers and microphones are recorded on a PC using a multichannel data acquisition system. The data has been analyzed for point mobility, average cylinder velocity and average sound pressure level in the chamber for each excitation location. Then the spatial average values of these parameters at all excitation locations are considered for the calculations.

The expression for the modal density of a structure is given in Ref. [9] as

$$n(f) = \frac{1}{(f_2 - f_1)} \int_{f_1}^{f_2} 4M \,\mathrm{Re}(Y)\,\mathrm{d}f, \tag{16}$$

where $\mathrm{Re}(Y)$ is the real part of point mobility and M is mass of the cylinder. The point mobility is the ratio between the velocity response of the structure measured at the excitation location and the force input to the cylinder.

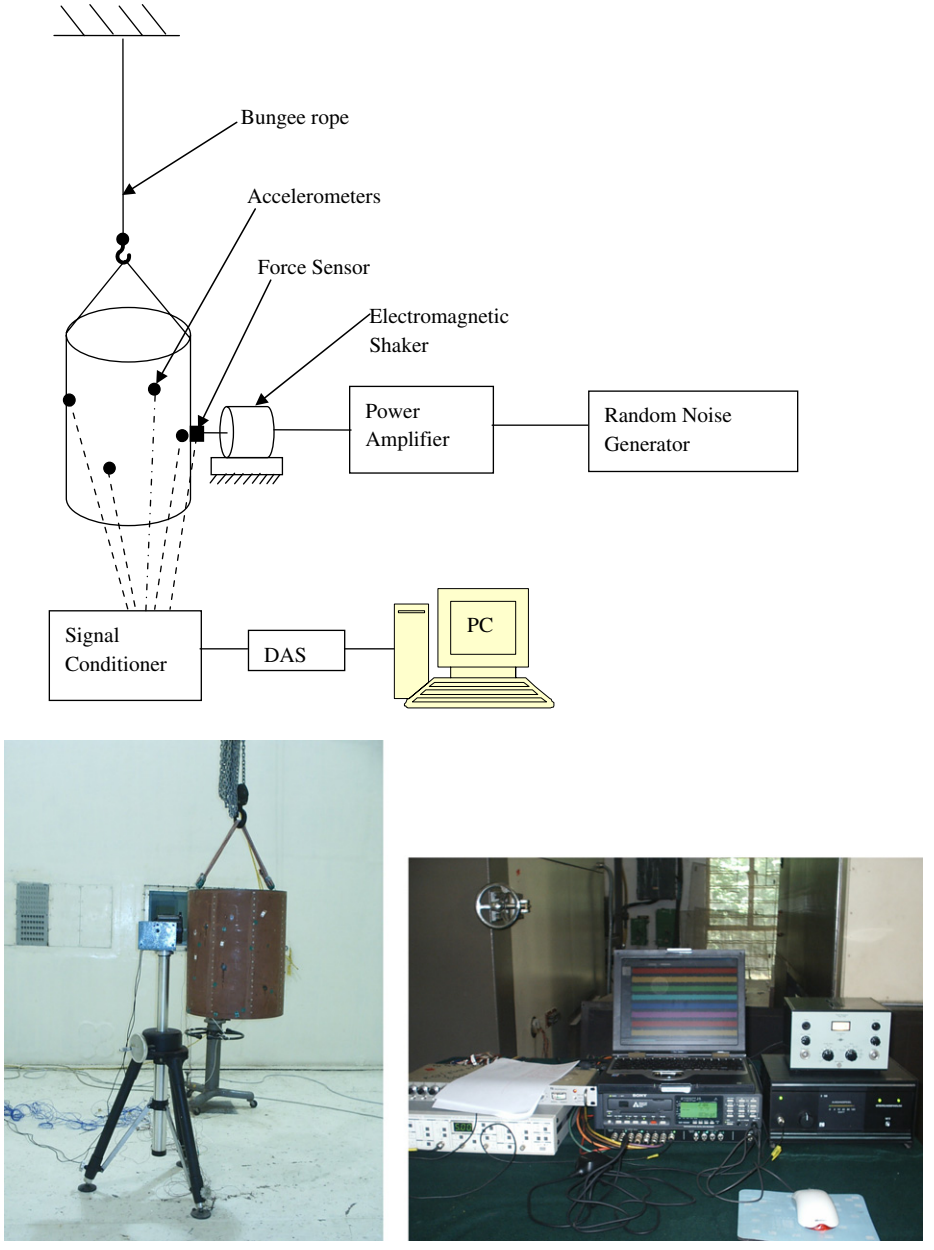

Fig. 10. Experimental setup.

3.1.1. *Unstiffened cylinder*

The predicted modal density of the unstiffened cylinder is compared with the measured modal density in Fig. 11. The bandwidth chosen for the analysis is 500 Hz. The measured modal density trend is similar to the predicted results and found to have good agreement. However, below the ring frequency of the unstiffened cylinder, the measured modal density is lower than the predicted values which may be due to several negative peaks in the point mobility plots because of very low damping of the structure. Also, below 2500 Hz, the difference in the measured and predicted modal densities may be due to different boundary conditions. Even though, in SEA, the boundary conditions may not be affecting the modal density, the cylinder considered in this case is short in length and hence the axial wavelengths are comparable with the cylinder length for the modes below the ring frequency. Xie et al. [27] demonstrated that the modal density of rectangular plate would

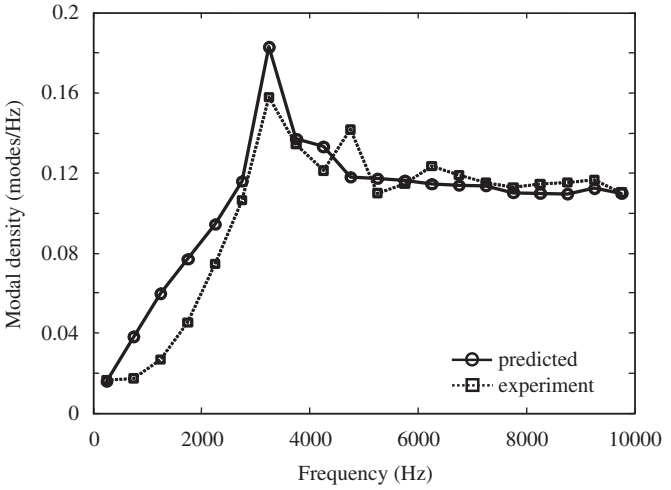

Fig. 11. Modal density of unstiffened cylinder.

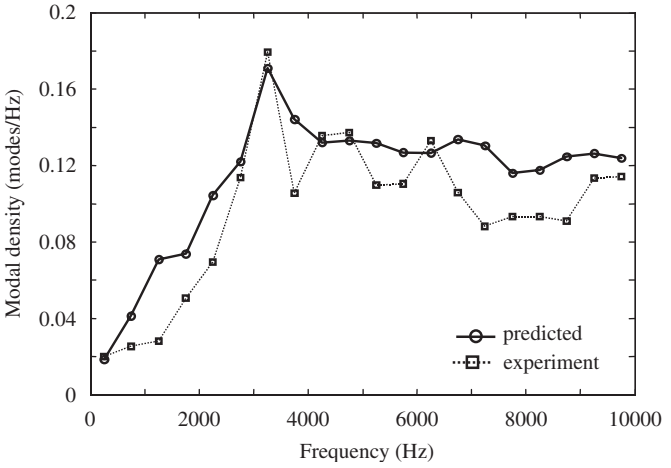

Fig. 12. Modal density of stiffened cylinder.

be depending upon the boundary conditions and could represent the true modal density only at high frequencies. Above, the ring frequency, the measured modal density agrees fairly well with analytical results. The variations in the measured modal density over the predicted values in this region can be minimized by either increasing the number of measurement locations or by increasing bandwidth to one-third octave bandwidth.

3.1.2. Stiffened cylinder

Fig. 12 compares the predicted and measured modal densities of stiffened cylinder with 8 'L'-type of stiffeners. The bandwidth assumed is 500 Hz as in the case of unstiffened cylinder. The measured modal density is lower than the predicted modal density for almost the entire frequency range. The lower values of measured modal density than the predicted values below 2500 Hz may be due to the reason explained for the unstiffened cylinder. Above the ring frequency, it has been seen that the variation in the modal density with different excitation locations are very high due to the local influence of the stiffeners and local modes predominate in this frequency region. Clarkson and Pope [9] pointed out the measured modal density was low

when the excitation point was nearer to the stiffeners and high when the excitation point was away from the stiffeners.

3.2. Radiation efficiency

Let us assume that the structure, the cylinder as system 1 and the surrounding acoustic volume, the reverberation chamber as system 2. Then the power balance equations of the two systems are

$$\pi_1 = \omega(\eta_1 + \eta_{12})E_1 - \omega\eta_{21}E_2, \tag{17}$$

$$\pi_2 = -\omega\eta_{12}E_1 + \omega(\eta_2 + \eta_{21})E_2, \tag{18}$$

where η_1 and η_2 are the DLFs of the cylinder and acoustic volume, η_{12} is the CLF between the cylinder and acoustic volume, E_1 and E_2 are the energies stored in the cylinder and acoustic volume and π_1 and π_2 are the power inputs to these systems. The CLF η_{21} between acoustic volume and the cylinder can be written as

$$\eta_{21} = \eta_{12}\left(\frac{n_1}{n_2}\right), \tag{19}$$

where n_1 and n_2 are the modal densities of the cylinder and acoustic volume, respectively. When the cylinder is given only mechanical excitation, Eq. (18) reduces to

$$\eta_{12} = \frac{n_2\eta_2 E_2}{(E_1 n_2 - E_2 n_1)} \tag{20}$$

and the radiation efficiency is calculated using Eq. (11). The modal density n_2 of acoustic volume is given by [25]

$$n_2 = \frac{4\pi f^2 V_2}{C^3} + \frac{\pi f A_2}{C^2} + \frac{P_2}{C}, \tag{21}$$

where P_2, A_2, V_2 are the total edge length, surface area and volume of the reverberation chamber. From the above equation, it can be seen that, the modal density of acoustic volume increases rapidly with frequency and hence $n_1 \ll n_2$ for the frequency $f > 100$ Hz. Hence, Eq. (20) can be simplified as

$$\eta_{12} = \frac{\eta_2 E_2}{E_1}. \tag{22}$$

The DLF of the chamber η_2 is given by

$$\eta_2 = \frac{13.816}{2\pi f T_{60}}, \tag{23}$$

where T_{60} is the reverberation time of the chamber. The energy E_1 of the cylinder is given by

$$E_1 = M\langle v_1^2\rangle, \tag{24}$$

where $\langle v_1^2\rangle$is the space averaged square of velocity of the cylinder, M the total mass of the structure. The energy E_2 of acoustic volume is given by

$$E_2 = \frac{\langle p_2^2\rangle V_2}{\rho_2 c^2}, \tag{25}$$

where $\langle p_2^2\rangle$ is the space average square of the sound pressure in the acoustic chamber and ρ_2 is the density of air.

3.2.1. Unstiffened cylinder

The measured CLF, η_{12} of the unstiffened cylinder is shown in Fig. 13 in one-third octave band frequencies. This bandwidth is chosen because the chamber reverberation time has been measured in one-third octave band only. The measured radiation efficiency using Eq. (10) is compared with the predicted values in Fig. 14 and the results agree to within a few percent. However, below 1600 Hz, there is a deviation between the predicted and measured radiation efficiency. This may be due to the different boundary conditions used for prediction and the measurements. Wang and Lai [18] pointed out that modal averaged radiation efficiency would depend

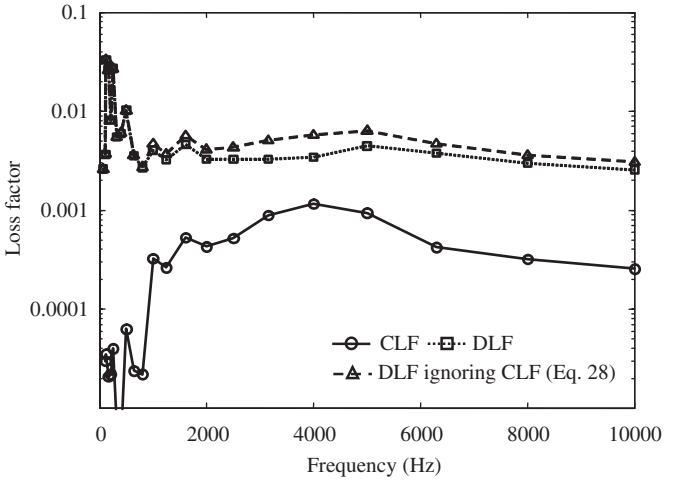

Fig. 13. Experimental loss factors of unstiffened cylinder.

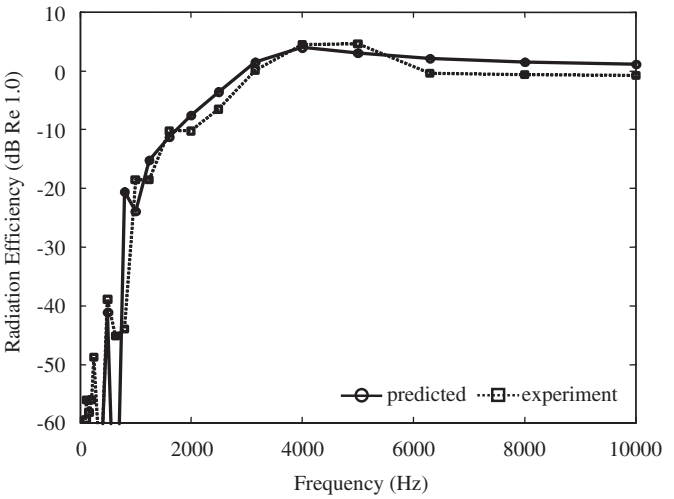

Fig. 14. Radiation efficiency of unstiffened cylinder.

upon the excitation and the boundary conditions and the variations of modal averaged radiation efficiency for cylindrical shell due to change of boundary conditions could be larger than that for a flat plate.

3.2.2. *Stiffened cylinder*

The measured CLF, η_{12} of the stiffened cylinder is given in Fig. 15 and the radiation efficiency in Fig. 16. The comparison of predicted and measured radiation efficiencies in Fig. 16 shows that measured efficiency is slightly less than the predicted results below the critical frequency as in the case of unstiffened cylinder. Above the ring frequency, there is not much difference between predicted and measured radiation efficiencies.

3.3. *Dissipation loss factor (DLF)*

Solving for η_1 from Eqs. (17) and (18), the DLF of cylinder is derived as

$$\eta_1 = \frac{P_{\text{in}}}{\omega E_1} - \frac{\eta_{12}}{E_1}\left\{\frac{\eta_2 E_1 - n_1 E_2}{n_2}\right\}. \tag{26}$$

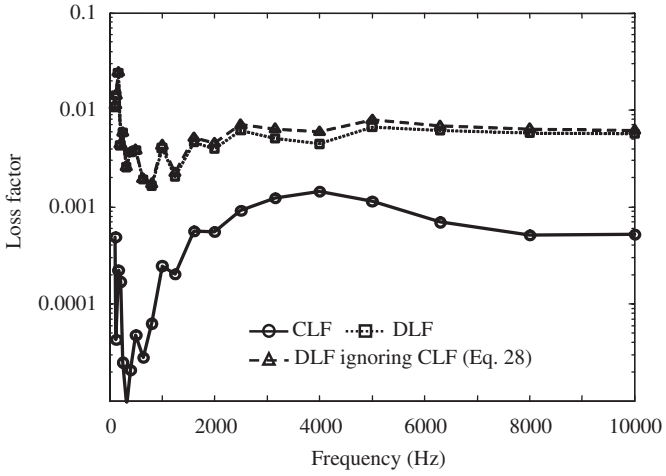

Fig. 15. Experimental loss factors of stiffened cylinder.

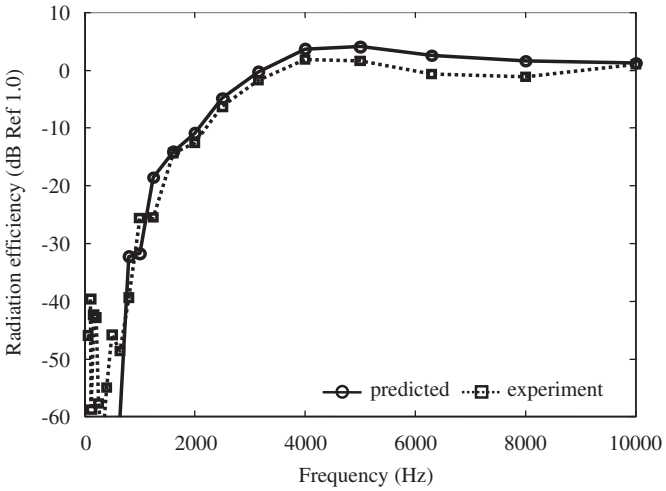

Fig. 16. Radiation efficiency of stiffened cylinder.

Since $n_1 \ll n_2$, Eq. (28) can be simplified to

$$\eta_1 = \frac{P_{\text{in}}}{\omega E_1} - \eta_{12}. \tag{27}$$

The CLF η_{12} will be an order of magnitude less than the DLF η_1 and usually it will be neglected and hence DLF is given as

$$\eta_1 = \frac{P_{\text{in}}}{\omega E_1}. \tag{28}$$

In most of the literatures [3,9,25,28], the DLF is calculated using Eq. (28) by neglecting the radiation damping. However, for thin structures, the radiation damping will be comparable with the DLF and hence Eq. (27) should be used for accurate estimation.

The DLFs of the unstiffened and stiffened cylinders are shown in Figs. 13 and 15, respectively. The DLF plots show fluctuations at low frequency due to predominant damping of individual global modes and vary from 0.002 to 0.03 for unstiffened cylinder and from 0.001 to 0.03 for stiffened cylinder. Above 3 kHz, DLF values are almost constant and their values are 0.004 and 0.006 for unstiffened and stiffened cylinders,

respectively. Ranky and Clarkson [28] estimated the average loss factor of uniform open-ended cylinder as 0.00219 from several tests by neglecting radiation damping as in Eq. (28).

3.4. Acoustic response of cylinders

Only the cylinders are suspended in the acoustic reverberation chamber and excited with acoustic noise in the band of 63 Hz to 10 kHz and acoustic tests are carried out separately for unstiffened and stiffened cylinders. 8 accelerometers were placed on the cylinders to measure the average velocity of the structure and 6 microphones were kept in the chamber to measure average sound pressure level. The one-third octave spectra of the acoustic excitations are shown in Fig. 17 and the overall sound pressure levels (OASPL) are 154.5 and 153.8 dB for unstiffened and stiffened cylinders, respectively. The acoustic spectra are having peak levels of 146.7 and 148.6 dB at 315 Hz one-third octave band. Above 2 kHz, there is a reduction in the acoustic levels with a roll-off of approximately 6 dB/octave. The spatially and spectrally averaged one-third band velocity spectra are shown in Figs. 18 and 19 for unstiffened and stiffened cylinders, respectively.

For the same acoustic levels as shown in Fig. 17, the vibration responses of unstiffened and stiffened cylindrical shells are predicted analytically using Eqs. (17) and (18). Substituting the values for the modal density, CLF and DLFs, these equations are solved for the cylinder energy E_1 from which the average (rms) response of the cylinder is calculated as

$$\langle v_1 \rangle = \sqrt{\frac{E_1}{M}}, \tag{29}$$

where M is the mass of the cylinder.

The predicted velocity response of the cylinder is compared with the measured velocity response in the same figures. For both the cylinders, the predicted and measured responses match well above the critical frequency but show significant deviation in the lower frequencies. At very low frequency, below 500 Hz, the modal density of the cylinders are very low and in this frequency region, SEA predictions are inaccurate. Between 500 Hz and 2 kHz, the radiation efficiencies of the structures are negligible and hence the predicted results are very sensitive to other parameters. Also, in this frequency region, the acoustic pressure difference between the cylinder interior and exterior acoustic volumes is less significant due to acoustic cross flow. The acoustic excitation forces acting on an open cylinder would be less than a covered cylinder. Hence, the prediction accuracy could be improved by treating the exterior and interior cylinder volumes as separate systems and covering both the ends of the cylinder in the experiment. Also, in this frequency region the predicted modal densities of the cylinders are higher than measured modal densities and hence the predicted responses would be slightly higher. Above the critical frequency, the predicted and measured acoustic responses of the cylinder

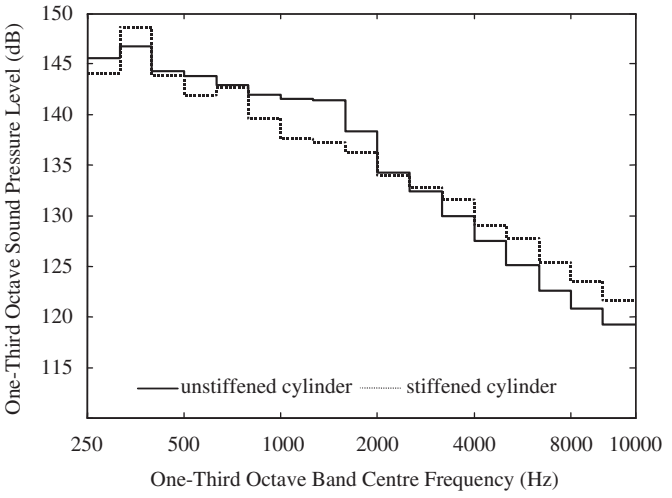

Fig. 17. One-third octave band sound pressure level of acoustic excitation.

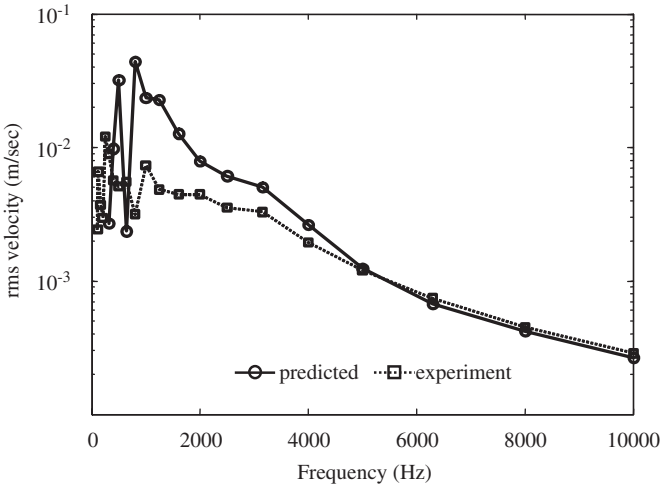

Fig. 18. Velocity response of unstiffened cylinder.

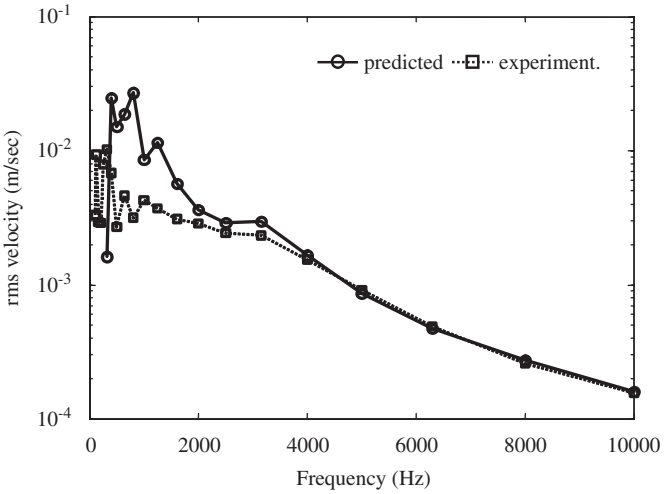

Fig. 19. Velocity response of stiffened cylinder.

match very well. In this frequency range, the variation between the predicted and measured modal density of the cylinders do not have much influence on the acoustic responses and the acoustic response curves show smooth variations with frequency. This may be due to very high modal density of the acoustic chamber, steady values of coupling and DLFs.

4. Conclusions

A simplified analytical method is presented in this paper to predict the two important SEA parameters, modal density and the radiation efficiency of longitudinally stiffened cylindrical shells. Both the parameters are calculated by solving a single eigenvalue problem of the structure. A statistical process has been introduced in the prediction by varying the geometrical and material properties by 5% with uniform distribution. First, the method has been validated for unstiffened cylinder for which analytical results are available in the literature. Next, the predicted value of modal density and the radiation efficiency of stiffened cylinders are verified experimentally by exciting the structure in a reverberation chamber using electrodynamic shaker.

The predicted results are found to have good agreement with experimental values except at low frequency, where the number of modes in the frequency band is less. A correction factor is applied to the predicted radiation efficiency below the critical frequency to accommodate for the radiation loss near the edges of unbaffled cylinder due to the acoustic short circuiting. A study has been conducted to assess the effect of the shape and the number of the stiffeners on these parameters keeping the total cross-sectional area of the stiffeners same. They have only small influence in the modal density and negligible influence in the radiation efficiency. As the number of stiffeners is increased beyond 32, the one term displacement field solution where the cross coupling of circumferential modes are neglected yields moderately accurate results. This simplifies the solution method and saves considerable computation time.

The vibro-acoustic response due to diffuse sound field is calculated through the SEA procedure using the predicted modal density and radiation efficiency values. The predicted response agrees well with experimental results especially above 4 kHz, the critical frequency of unstiffened cylinder. At low frequencies the agreement is not good as is usually the case in the SEA prediction. The present method can also be extended to predict the vibro-acoustic response of non-periodically stiffened cylinders or stiffeners with different cross-sections.

References

[1] J.P.D. Wilkinson, Modal densities of certain shallow structural elements, *Journal of the Acoustical Society of America* 43 (1967) 245–251.

[2] L. Cremer, M. Heckl, E.E. Ungar, *Structure-Borne Sound*, Springer, Berlin, 1988.

[3] R.H. Lyon, *Statistical Energy Analysis of Dynamical Systems*, MIT Press, Cambridge, MA, 1975.

[4] E. Szechenyi, Modal densities and radiation efficiencies of unstiffened cylinders using statistical method, *Journal of Sound and Vibration* 19 (1971) 65–81.

[5] G.H. Elliott, The evaluation of modal density of paraboloidal and similar shells, *Journal of Sound and Vibration* 126 (1988) 477–483.

[6] R.S. Langley, The modal density and mode count of the thin cylinders and curved panels, *Journal of Sound and Vibration* 169 (1994) 43–53.

[7] S. Finnvedan, Formulas for modal density and for input power from mechanical and fluid point sources in fluid filled pipes, *Journal of Sound and Vibration* 208 (1997) 705–728.

[8] G. Maymon, Modal densities of stiffened, axially loaded cylindrical shells, *Journal of Sound and Vibration* 42 (1975) 115–127.

[9] B.L. Clarkson, R.J. Pope, Experimental determination of vibration parameters required in the statistical energy analysis method, *Journal of Vibration, Acoustics, Stress and Reliability in Design* 105 (1983) 337–344.

[10] F.W. Williams, J.R. Banerjee, Accurately computed modal densities for panels and cylinders including corrugations and stiffeners, *Journal of Sound and Vibration* 93 (1984) 481–488.

[11] R.S. Langely, On the modal density and energy flow characteristics of periodic structures, *Journal of Sound and Vibration* 172 (1994) 491–511.

[12] S. Finnveden, Evaluation of modal density and group velocity by a finite element method, *Journal of Sound and Vibration* 273 (2004) 51–75.

[13] J.E. Manning, G. Maidanik, Radiation properties of cylindrical shells, *Journal of the Acoustical Society of America* 36 (1964) 1691–1698.

[14] F. Fahy, *Sound and Structural Vibration, Radiation, Transmission and Response*, Academic Press, London, 1985.

[15] M.C. Junger, D. Feit, *Sound, Structures and Their Interaction*, MIT Press, Cambridge, MA, 1986.

[16] P.R. Stepanishen, Radiated power and radiation loading of cylindrical surfaces with non-uniform velocity distribution, *Journal of the Acoustical Society of America* 63 (1978) 328–338.

[17] P.R. Stepanishen, Modal coupling in the vibration of fluid loaded cylindrical shells, *Journal of the Acoustical Society of America* 71 (1982) 813–823.

[18] C. Wang, J.C.S. Lai, The sound radiation efficiency of finite length acoustically thick circular cylindrical shells under mechanical excitation I: Theoretical analysis, *Journal of Sound and Vibration* 232 (2000) 431–447.

[19] B. Laulagnet, J.L. Guyader, Sound radiation by finite cylindrical ring stiffened shells, *Journal of Sound and Vibration* 138 (1990) 173–191.

[20] D.J. Mead, N.S. Bardell, Free vibration of thin cylindrical shells with discrete axial stiffeners, *Journal of Sound and Vibration* 111 (1986) 229–250.

[21] D.M. Eagle, J.L. Sewalll, An analysis of free vibration of orthogonally stiffened cylindrical shells with stiffeners treated as discrete elements, *AIAA Journal* 6 (1968) 518–526.

[22] P. Ramachandran, S. Narayanan, Modal density of stringer stiffened cylindrical shell structure, *International Conference on Theoretical, Applied, Computational and Experimental Mechanics (ICTACEM 2004)* IIT, Kharaghpur, India, December 28–30, 2004.

[23] X.L. Huang, C.J. Radcliffe, Probability distribution of statistical energy analysis model responses due to parameter randomness. *ASME-JVA*, 1997, pp. 1–6.

[24] V.R. Miller, L.L. Faulkner, Prediction of aircraft interior noise using the statistical energy analysis method, *Journal of Vibration, Acoustic, Structure and Reliability in Design* 105 (1983) 512–518.
[25] N.C. Nigam, S. Narayanan, *Applications of Random Vibration*, Narosa, India, 1994.
[26] C.H. Oppenheimer, S. Dubowsky, A radiation efficiency for unbaffled plates with experimental validation, *Journal of Sound and Vibration* 199 (1997) 473–489.
[27] G. Xie, D.J. Thomson, C.J.C. Jones, Mode count and modal density of structural systems: relationship with boundary conditions, *Journal of Sound and Vibration* 274 (2004) 621–651.
[28] M.F. Ranky, B.L. Clarkson, Frequency average loss factors of plates and shells, *Journal of Sound and Vibration* 89 (1983) 309–323.